Fuel 314 (2022) 122768

Contents lists available at ScienceDirect

Fuel

journal homepage: www.elsevier.com/locate/fuel

Full Length Article

Performance and sensitivity analysis of packed-column absorption process using multi-amine solvents for post-combustion CO_2 capture

Hyun-Taek Oh [a], Jae-Cheol Lee [b], Chang-Ha Lee [a,*]

[a] Department of Chemical and Biomolecular Engineering, Yonsei University, Seoul, Republic of Korea
[b] AVEVA Korea Ltd., Seoul, Republic of Korea

ARTICLE INFO

Keywords:
Post-combustion CO_2 capture
Multi-amine
Energy reduction
Rate-based model
Sensitivity analysis

ABSTRACT

Although many novel multi-amine solvents with high CO_2 solubility were reported, they have not yet been evaluated for the performance in CO_2 absorption processes. In this study, the efficiency and inside profile of the packed-column CO_2 absorption process using a novel multi-amine solvent were investigated by using a mathematical model. Three amine solvents were selected: 2-(2-aminoethylamino)-ethanol (AEEA) and diethylenetriamine (DETA) as multi-amine solvents and monoethanolamine (MEA) as a reference. Based on the 90% capture efficiency of flue gas CO_2 from a coal-fired power plant, a sensitivity analysis using the liquid-to-gas ratio was conducted to minimize the energy consumption for CO_2 capture. Based on the utilization of the same 30 wt% solvent, the lowest reboiler thermal energy achieved by the process using DETA was 3.242 GJ/tonCO_2, which was 8.57% lower than that obtained when MEA was employed. In contrast, the process using AEEA required 7.04% higher energy than MEA. In the process modified by rich-solvent split for further enhancing efficiency, the DETA process could achieve 2.962 GJ/tonCO_2, which reduced the reboiler duty by 16.8% from the MEA process. The CO_2 capture performance of absorbents could not be evaluated not only by the absorption rate and capacity. Owing to the larger molecular weight of multi-amines than MEA, the performance of capture and regeneration was discussed with respect to the amine properties and number of amine moles in the solution. A well-selected multi-amine for a modified process configuration has considerable potential for improving the energy efficiency of CO_2 capture.

1. Introduction

Power generation via fossil fuel-fired power plants is regarded as the largest single source of CO_2 emissions [1]. Carbon capture and storage technologies remain critical solutions for rapid CO_2 emission reduction. Compared with other carbon capture technologies, the solvent absorption process is the most applicable mature technology for large-scale CO_2 capture [1,2].

The solvent using commercial scale CO_2 capture technologies can be divided into two categories; chemical and physical solvent. The chemical solvents achieve CO_2 capture by reactions while the physical solvents dissolve CO_2 without reactions. Therefore, temperature is one of the key operating variables in chemical absorption processes, but pressure is an important operating variable in physical absorption processes [3]. Alternatively, it was also reported that dry solid sorbents has high potential for CO_2 capture [4]. However, the further enhancement of the sorption rate, stability, and/or particle size control for many advanced solid sorbents is required for practical applications [5,6].

The CO_2 capture process using a physical solvent is widely accepted for an integrated gas turbine combined cycle (IGCC) power plant as a pre-combustion CO_2 capture [7,8]. However, in post-combustion CO_2 capture, the chemical solvent absorption process is a commercially available competitive technology for fossil fuel-fired power plants [9,10]. Since a substantial amount of energy is required for chemical solvent regeneration [11,12], various configurations for absorption process have been developed to reduce high energy demand [13,14]. The rich-solvent split (RSS) modification for absorption processes could enhance energy efficiency. In addition, since the RSS modification does not need additional devices, the modified configuration of the absorption process is relatively simple and the capital cost is cheap compared with other modifications [13].

Commercially available monoethanolamine (MEA), a representative primary amine, has been widely applied to the absorption process for CO_2 capture. However, MEA is not enough to achieve efficient and economical CO_2 capture due to high energy consumption in absorption

* Corresponding author.
E-mail address: leech@yonsei.ac.kr (C.-H. Lee).

https://doi.org/10.1016/j.fuel.2021.122768
Received 24 July 2021; Received in revised form 17 November 2021; Accepted 28 November 2021
Available online 9 December 2021
0016-2361/© 2021 Elsevier Ltd. All rights reserved.

Nomenclature

Upper case

A_e	effective area (m^2/m^3)
C_t^j	molar concentration in phase j (mol/m^3)
$C_{p,i}$	heat capacity of component i (J/kmol-K)
D_j	diffusivity in phase j (m^2/s)
E_1	enhancement factor of a pseudo-first-order reaction (-)
E_∞	instantaneous reaction (-)
E_{CO_2}	enhancement factor (-)
H	Henry's constant (-)
P	pressure (Pa)
P_i^{sat}	saturated pressure of component i (Pa)
P_i^v	partial pressure of component i (Pa)
$Q_{desorption}$	heat of desorption (W)
Q_{latent}	latent heat (W)
$Q_{reboiler}$	reboiler duty (W)
$Q_{sensible}$	sensible heat (W)
R	ideal gas constant (8.314 J/mol-K)
S	side dimension of corrugation (m)
T	Temperature (K)
V_i	molar volume of component i (cm^3/mol)

Greek letters

ΔH_{ab}	heat of absorption (J/mol)
$\Delta H_{evap,i}$	enthalpy of vaporization of component i (J/mol)
α	CO_2 loading in amine (CO_2 mole flow rate in solvent / amine mole flow rate in solvent)
ρ_j	density in phase j (kg/m^3)
μ_i	viscosity of component i (cP)

Lower case

a,b,c,d	parameters of the VLE empirical equations (-)
c_1, c_3	parameters of the properties empirical equations (-)
c_2, c_4	parameters of the properties empirical equations (K)
h_L	fractional holdup of liquid (-)
h_{ov}	heat transfer coefficient (J/m^2-K)
$k_{2,i}$	second-order rate constant of component i (m^3/kmol-s)
k_i^j	mass transfer coefficient of component i in phase j (mol/Pa-s-m^3)
k_v	thermal conductivity (W/m-K)
n	mass transfer rate (mol/s)
u_{je}	effective velocity in phase j (m/s)
x_i	mole fraction of component i in liquid phase (-)
y_i	mole fraction of component i in vapor phase (-)

processes. Therefore, considerable efforts have been devoted to the development of advanced amine solvents, which have been reported to have higher CO_2 capture capacity than MEA [15,16].

Primary and secondary amines are known to have fast reaction rates and high heat of absorption. In contrast, tertiary amines are known to have a slow reaction and low heat of absorption [17]. Primary and secondary amines mainly have two amine molecules that can react with one CO_2 molecule; hence, a CO_2 loading exceeding 0.5 mol CO_2/mol amine is difficult to achieve. On the contrary, one tertiary amine molecule can react with one CO_2 molecule [18]. Accordingly, many studies have developed solvent blends of primary, secondary, and tertiary amines to supplement their strengths and weaknesses [15,19]. Different from solvent blends, multi-amines have several amine groups in one molecule. It was reported that some multi-amines could achieve a CO_2 loading exceeding 1.0 mol CO_2/mol [20]. In addition, multi-amines with primary and secondary amine groups exhibited high reaction rates with CO_2.

Many studies have concentrated on measuring and modelling the properties and solubility of CO_2 in various advanced and blended absorbents [21,22]. In addition, the absorption rates and capacities of absorbents have widely been reviewed [20,23]. On the other hand, only limited absorbents have been evaluated with respect to the efficiency evaluation of absorption processes using newly developed absorbents. Furthermore, few studies for the absorption process using multi-amines is rarely investigated even though the high performance of their absorption capacity and rate were reported. There is a great knowledge gap between the properties of absorbents and the performance of processes using advanced amine solvents because energy consumption mainly occurs in regeneration. Therefore, the feasibility and reliability of multi-amines should be evaluated again in absorption processes regardless of their high absorption rate and capacity.

In this study, the performance and sensitivity of the CO_2 absorption process employing multi-amines were evaluated through a rate-based model. The detailed inside phenomena in the absorption process was elucidated to establish the relationship between performance and operating variables. Two multi-amines were selected: 2-(2-aminoethylamino)-ethanol (AEEA) with two amine groups and diethylenetriamine (DETA) with three amine groups as the representative multi-amines because the properties of these two multi-amines were well established as shown in Table 1, compared with other multi-amines. Therefore, the assumptions and uncertainty to simulate the absorption process, resulting from the multi-amines' properties, could be minimized. The absorption process using MEA was selected as a reference to compare the performance and energy efficiency with the processes using the multi-amines. However, multi-amines with tertiary amine groups were not selected because of their slow reaction rates.

Both of selected multi-amines contain primary and secondary amine groups; hence, the reaction with CO_2 can be faster than MEA. However, the information of absorption capacity and rate of absorbents is not sufficient to evaluate the capture efficiency and energy consumption of the absorption process because the cyclic absorption process is operated with an absorber and a stripper. Therefore, the efficiency of the absorption process must be evaluated in detail with respect to the mutual effect of multi-amines on absorption and stripping. Since the comparison was based on the same 30 wt% solvent, the effect of number of amine groups on the performance of the absorption process was also studied.

A rate-based model of the absorption process was use to simulate the capture process, incorporating the equations for vapor–liquid equilibrium (VLE), reaction heat, physical properties, mass transfer, and reaction rate. The rate-based model used in the study was validated with reference to the pilot data of MEA [10,38,39]. In this study, the CO_2 capture efficiency was defined as the ratio of the flow rate of CO_2 produced from a stripper to that supplied from the flue gas. The reboiler duty was determined to achieve 90% of CO_2 capture efficiency because many previous studies reported a minimum energy penalty at this capture efficiency [40–42]. Then, as an important operating parameter, the effect of the liquid-to-gas (L/G) ratio on energy efficiency was investigated based on a 90% CO_2 capture efficiency. The energy consumption analysis was categorized based on the latent heat of H_2O, CO_2 desorption, and sensible heat.

Since the properties of AEEA, DETA and MEA are very different, it was expected that the enhancement by the absorption process modification could be different among the solvents. Therefore, the feasibility of enhancing the energy efficiency of the absorption process using each solvent was also evaluated by modifying the configuration with RSS. Finally, the potential improvements for the absorption process with multi-amines were suggested to increase the energy efficiency of CO_2 capture.

Table 1
Physical and chemical properties of amines used in this study [24–37].

Amine	MEA	AEEA	DETA
IUPAC name	Monoethanolamine	2-(2-Aminoethylamino)-ethanol	Diethylenetriamine
Chemical formula	$H_2NCH_2CH_2OH$	$H_2N(CH_2)_2NH(CH_2)_2OH$	$HN(CH_2CH_2NH_2)_2$
Molecular structure	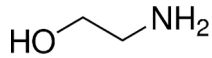	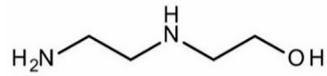	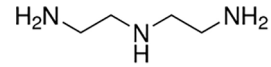
Pure amine properties			
Molecular weight [g/mol]	61.08	104.15	103.17
Density at 313.15 K [g/cm^3], [25–27]	1.0000	1.014	0.9338
Viscosity at 313.15 K [cP], [26–28]	9.61	39.4	3.4001
Heat capacity at 313.15 K [J/mol-K], [29–31]	170.25	284.55	275.43
Amine (30 wt%) + Water (70 wt%) Mixture properties			
Density at 313.15 K [g/cm^3], [25–27]	1.0035	1.0151	1.0043
Viscosity at 313.15 K [cP], [26–28]	1.67	2.29	2.68
Heat capacity at 313.15 K [J/mol-K], [29–31]	78.969	104	101.8
CO_2 loading at 313.15 K and 15 kPa [mole CO_2/mole amine], [32–34]	0.580	0.806	1.240
Henry's constant at 313.15 K, [35]	4,256	4,766	5,309
Second order reaction rate (k2) at 313.15 K [m^3/kmol-s], [36–38]	6,533	22,674	90,880

2. Methodology

2.1. Process description

The operational results from a CESAR pilot plant using MEA (Tests 1A-1–1A-4) were selected to validate the simulation and used as comparative reference [10,38]. The CESAR pilot plant was operated on a slipstream of flue gas from the Dong Esbjerg power station (a 400-MW pulverized bituminous coal power plant). This conventional process using MEA consists of an absorber, a stripper, and a rich/lean solvent heat exchanger, as shown in Fig. 1. The process could capture 90% of the incoming carbon in the flue gas at a rate of 5000 Nm^3/h. The operating and process conditions for model validation are listed in Table 2.

The absorber and stripper consist of a packing section and a water-washing section. The packing section begins at the bottom of the tower, and the water-washing section is located at the top to reduce amine emissions; the amine solvent was supplied between these two sections. The lean amine solvents were cooled to 313.15 K by a rich/lean amine heat exchanger and cooler. The minimum temperature in the heat exchanger used in this study was assumed to approach 6 K; other process specifications were identical to those used in a previous study [13].

The same absorption process (Fig. 1) was applied to other multi-amines (i.e., AEEA and DETA). A comparative study indicates that the mass concentrations of AEEA and DETA are the same as that of MEA (30 wt% solution), as summarized in Table 1. Regardless of the amine type, all the absorption processes were studied to minimize the energy consumption under the condition that the CO_2 removal efficiency was to exceed 90%.

2.2. Modeling of thermodynamic properties

The physical properties of the amine solvents used in this study were calculated using an empirical equation and/or equation of state (EOS). Because physical properties are important factors in determining the accuracy of the absorption model, the estimated physical properties were verified using data published in the literature.

In this study, the saturated pressure for VLE was calculated using a simplified empirical equation (Eq. (1)). The heat of absorption is calculated using the Gibbs–Helmholtz equation combined with a simplified VLE empirical model (Eq. (2)) [31]. The saturated vapor

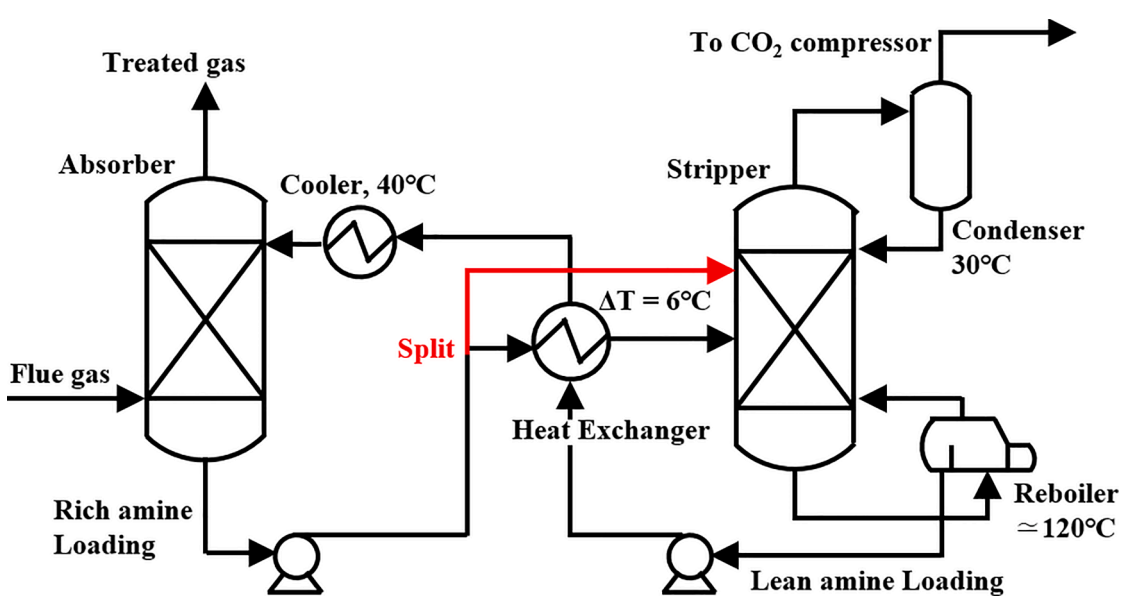

Fig. 1. Schematic of absorption process for CO_2 capture (red line indicates RSS). (For interpretation of the references to colour in this figure legend, the reader is referred to the web version of this article.)

Table 2
Operating conditions of process using MEA (reference) [10,38].

Feed specification	Flue gas	Lean MEA solvent	Rich MEA solvent
Temperature [℃]	49.07	40	49.64
Pressure [bar]	1.1	1.1	1.05
Flow rate [Nm^3/hr]	4974.92	529.39	523.77
Compositions			
N_2	0.755	–	–
O_2	0.03	–	–
H_2O	0.105	0.8684	0.8273
CO_2	0.11	0.0219	0.0618
MEA	–	0.1096	0.1109
Process conditions			
	Absorber	Stripper	
Height [m]	17, 3[a]	10, 3[a]	
Diameter [m]	1.1, 1.1[a]	1.1, 0.8[a]	
Pressure [bar]	1.05	1.87	
Packing type	Sulzer Mellapak 2X	Sulzer Mellapak 2X	

[a] For water washing section.

pressure of H_2O for VLE was calculated using Antoine equation (Eq. (3)). In this study, since the activity coefficient was assumed as 1.0, the mass transfer direction of H_2O was determined to satisfy Raoult's law. It was assumed that N_2 and O_2 were not involved in mass transfer between the liquid and vapor phases.

$$ln(P_i^{sat}) = a + bT + (cT + d)\alpha \tag{1}$$

$$\Delta H_{ab} = R\frac{dln(P_i^{sat})}{d(1/T)} = RT^2(b + c\alpha) \tag{2}$$

$$log_{10}(P_i^{sat}) = a - \frac{b}{c + T} \tag{3}$$

where P_i^{sat} is the saturated pressure of component i; a, b, c, and d are the parameters of the VLE empirical equation; α is the CO_2 loading in amine (CO_2 mole flow rate in solvent per amine mole flow rate in solvent); T is the amine solvent temperature; ΔH_{ab} is the heat of absorption; and R is the gas constant.

To improve the accuracy of the model, the parameters were obtained at two temperature ranges. First, the model was fitted to the VLE experimental data, and the heat of absorption was in the range 313.15–353.15 K, which was the operating temperature range of the absorber. Furthermore, in the post-combustion CO_2 capture process using amines, the partial pressure of CO_2 was generally maintained below 20,000 Pa inside the absorber. Therefore, the experimental VLE data obtained at a pressure of less than 20,000 Pa were also used to obtain the parameters. Second, the parameter set was obtained from the experimental data in the range 353.15–393.15 K, which was the operating temperature range of the stripper. In the stripper, because the partial pressure of CO_2 was generally operated at 100,000 Pa or less, the parameters were fitted using experimental VLE data obtained at a pressure of less than 100,000 Pa.

Fig. 2 shows that the thermodynamic model could reasonably predict the experimental CO_2 partial pressure and heat of absorption versus CO_2 loading in DETA and AEEA. The VLE empirical model parameters for Eq. (1) that have been obtained by fitting the VLE experimental data for each solvent are listed in Table 3. And the parameters of Antoine equation for water in Eq. (3), which were obtained from the Dortmund Data Bank (DDBST), are also listed in Table 3.

The simplified model in Eq. (1) showed 4.74% and 4.33% deviations in the CO_2 loading prediction for DETA and AEEA solvent, respectively, in the operating temperature range of the absorber in the study. In the operating temperature range of the stripper, the prediction deviations of

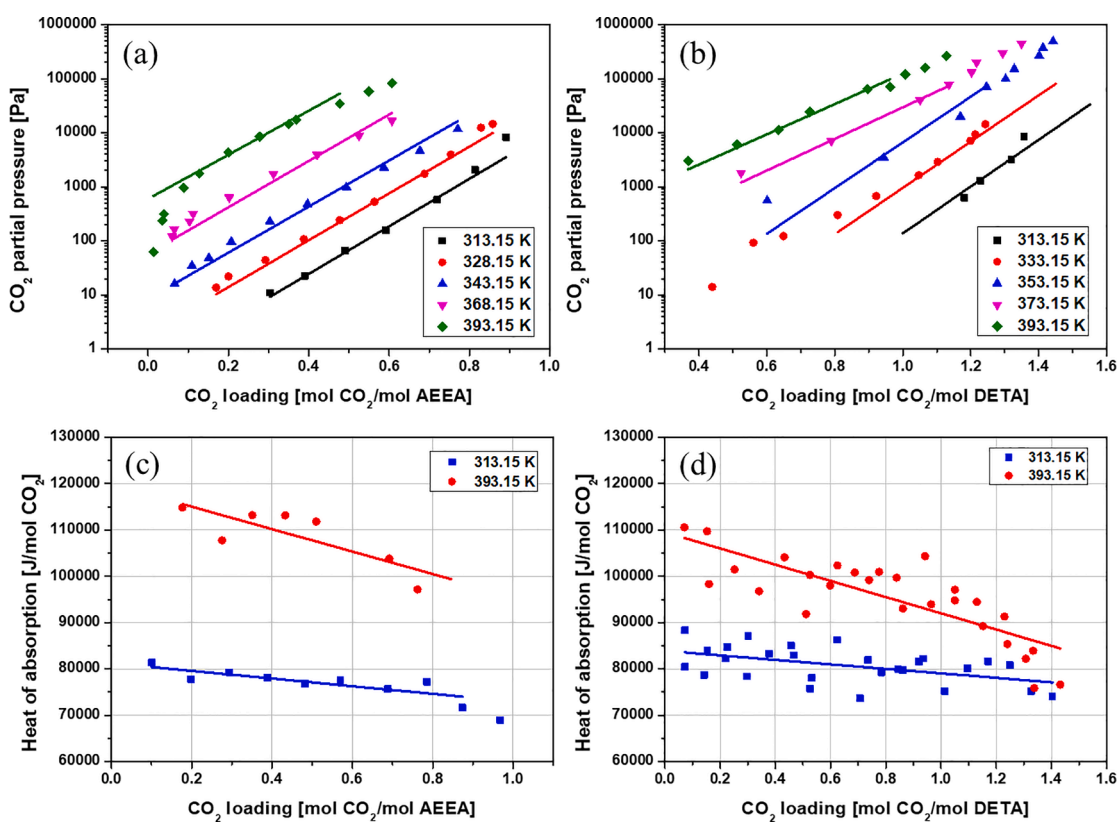

Fig. 2. Comparison of experimental data with predicted CO_2 partial pressure and heat of absorption versus CO_2 loading using two different amine solvents: CO_2 partial pressure in (a) AEEA [32] and (b) DETA [31], Heat of absorption of (c) AEEA [43] and (d) DETA [44].

Table 3
Parameters of VLE empirical equation for each amine solvent [31–33,43,44].

	a	b	c	d	Ref. of Exp. Data
MEA (absorber)	−35.98	0.1053	−0.0047	21.71	[34,43]
MEA (stripper)	−30.32	0.0909	−0.0196	24.86	
DETA (absorber)	−37.27	0.1029	−0.0060	11.83	[32,44]
DETA (stripper)	−28.24	0.0852	−0.0136	11.82	
AEEA (absorber)	−32.06	0.0997	−0.0102	13.31	[33,43]
AEEA (stripper)	−30.28	0.0933	−0.0188	16.80	
H_2O	10.1962	1730.63	−39.724		DDBST

DETA and AEEA solvent were 4.01 % and 5.96 %, respectively. A certain deviation between the calculated and predicted CO_2 partial pressures was observed at the low and high CO_2 loadings of AEEA (Fig. 2(a)) and at the highest temperature (393.15 K). This was because the saturated pressure of the solvent significantly changed with the CO_2 loading on a logarithmic scale. The heat of absorption exhibits an average deviation of less than 4%, as shown in Fig. 2, (c) and (d). Considering the prediction results from the rigorous reaction equilibrium model using 11 reaction equilibrium constants for AEEA [43] and 19 reaction equilibrium constants for DETA [44], the simplified model was comparative in the operation range in the study. However, the rigorous reaction equilibrium model can give more accurate VLE prediction if the absorption process configuration or operational range is different from this study.

The physical properties used in this study were separately calculated for the liquid and vapor phases. The liquid-phase physical properties, such as density, viscosity, heat capacity, vapor pressure, heat conductivity, Henry's constant, and second-order reaction rate constant, were calculated using empirical equations based on a mixing rule. The mixing rule-based empirical equations (Eqs. (3)–(6)) were used to calculate the liquid phase properties for each amine. And Eq. (7) was used to calculate Henry's constant between each amine solvent and CO_2 in the vapor phase. The parameters of the physical property equations (c_1 to c_4) are listed in Table 4.

In the vapor phase, the properties (H_2O, CO_2, N_2 and O_2) were calculated using the Redlich–Kwong EOS. However, since the amine concentration in the vapor phase was extremely low, its concentration was neglected. The physical properties of each pure component were obtained from the National Institute of Standards and Technology [45]. The mixing rule-based empirical equations and parameters used to calculate the liquid phase properties for each amine are as follows:

$$V_{mix} = V_{H_2O}x_{H_2O} + V_{amine}x_{amine} + (c_1 + c_2/T)x_{H_2O} + (c_3 + c_4/T)x_{amine} \quad (4)$$

$$ln\mu_{mix} = \sum_{i=1}^{2} x_i ln\mu_1 + \sum_{i=1}^{2}\sum_{j=i+1}^{2}(k_{ij}x_ix_j + m_{ij}x_i^2x_j^2) \quad (5)$$
$$k_{ij} = c_1 + c_2/T,\ m_{ij} = c_3 + c_4/T$$

$$C_{p,mix} = C_{p,H_2O}x_{H_2O} + C_{p,amine}x_{amine} + (c_1 + c_2/T)x_{H_2O} + (c_3 + c_4/T)x_{amine} \quad (6)$$

$$\ln H_{amine-CO_2} = c_1 + c_2/T + c_1\ln T + c_4T \quad (7)$$

where subscript i represents the liquid species (amine, H_2O, or amine solvent); x is the mole fraction in the liquid phase; V is density; μ is viscosity; C_p is the heat capacity; and H is Henry's constant.

Fig. 3 shows the predicted density, viscosity, and heat capacity versus temperature for three different amines (i.e., MEA, DETA, and AEEA) and compares them with the experimental data. The experimental heat capacity of AEEA showed non-linear variation (S-shape) within a small range of temperature, the variation of which was hard to find in other various amines within such a small temperature range. On the other hand, the predicted result by the mixing rule-based empirical equation (Eq. (6)) was almost linear, and the Redlich-Kister equation with reference parameters also showed a very similar result as Eq. (6). The deviation from the experimental heat capacity in AEEA was 2.1% while the other calculated properties showed an average deviation of only 1% from the experimental data.

To calculate the chemical absorption rate, a termolecular mechanism is applied, assuming that the reaction occurred in a single step [46].

$$CO_2 + RNH_2 + H_2O \longleftrightarrow {}^{k_{H_2O}}{}_{k_{-H_2O}} RNHCOO^- + H_3O^+ \quad (8)$$

$$CO_2 + 2RNH_2 \longleftrightarrow {}^{k_{Am}}{}_{k_{-Am}} RNHCOO^- + RNH_3^+ \quad (9)$$

According to this mechanism, the forward reaction rate could be expressed as

$$r_{CO_2} = (k_{Am}[RNH_2] + k_{H_2O}[H_2O])[RNH_2][CO_2] \quad (10)$$

$$r_{CO_2} = k_{obs}[CO_2] \quad (11)$$

$$k_{obs} = k_2[RNH_2] \quad (12)$$

$$k_{obs} = (k_{Am}[RNH_2] + k_{H_2O}[H_2O])[RNH_2] \quad (13)$$

where k_{Am} is the reaction rate constant resulting from the use of amine; k_{H_2O} is the reaction rate constant by H_2O; k_{obs} is the observed reaction rate constant; and k_2 is the second-order rate constant.

Eqs. (12) and (13) represent the reaction rate constants for CO2 and each amine solvent where the reactions of Eqs. (8) and (9) were considered. The observed reaction rate constants (k_{obs}) for MEA and AEEA were calculated using Eq. (12), and that for DETA was obtained from Eq. (13). The second-order rate constants for MEA and AEEA (k_2 in

Table 4
Parameters of physical property equations for each amine solvent [24–30,34].

Property		c_1	c_2	c_3	c_4	Ref. of Exp. Data
Density	MEA	−0.0584	31.37	−0.771	−432	[25]
	DETA	−0.3512	143.40	−6.672	−1737	[26]
	AEEA	−0.0847	41.09	−2.170	−1251	[27]
Viscosity	MEA	−6.19	4046	4.58	−3915	[28]
	DETA	−20.90	13,290	−138.30	37,340	[26]
	AEEA	−22.65	12,110	−24.18	3673	[27]
Heat capacity	MEA	−4.719e4	1.976e7	−9.509e3	8.377e5	[29]
	DETA	3.530e5	−9.376e7	8.503e2	−5.094e7	[30]
	AEEA	3.058e5	−9.145e7	1.795e5	−5.393e7	[31]
Henry's constant	MEA	−4171.0	113,531	726.45	−1.1428	[35]
	DETA	−1196.0	31,653	210.27	−0.3348	[35]
	AEEA	2021.1	−59079	−345.66	0.5187	[35]

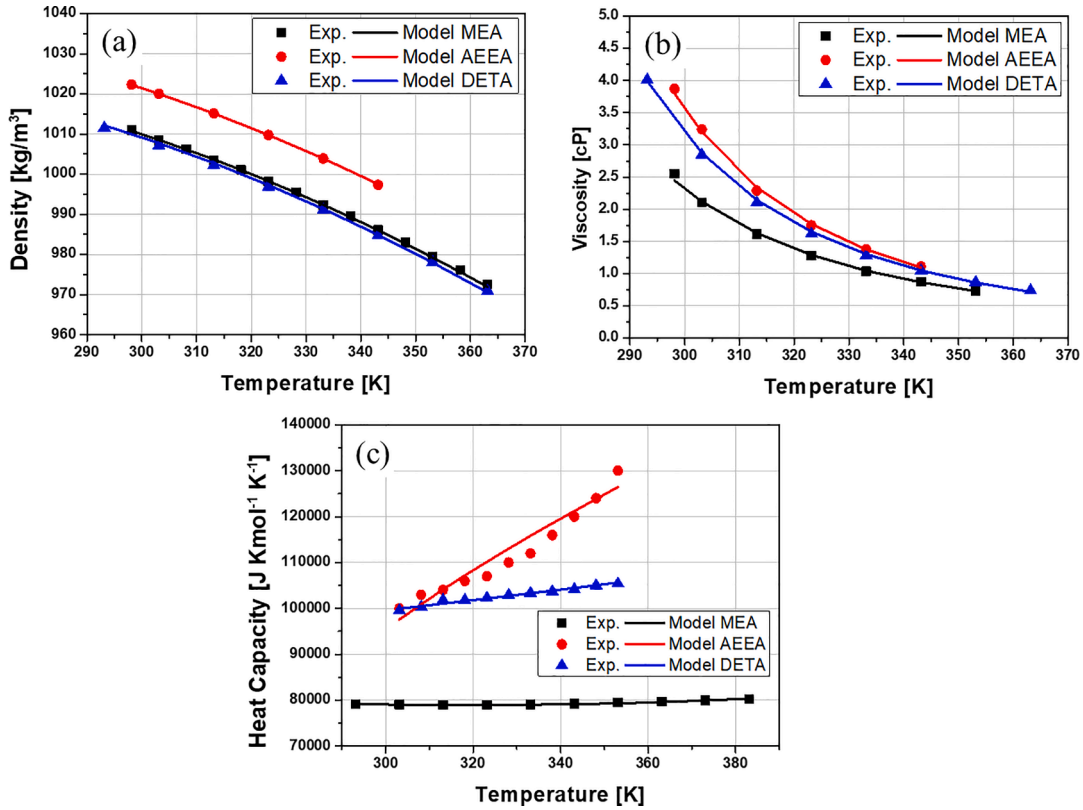

Fig. 3. Comparison of experimental data with predicted physical properties versus temperature in three different amine solvents: (a) Density [24–26], (b) Viscosity [25–27], (c) Heat capacity [28–30].

Eq. (12)) and the reaction rate constants by amine and H_2O for DETA (k_{Am} and k_{H_2O} in Eq. (13)) were calculated by Eqs. (14)-(16) for MEA [35], DETA [36] and AEEA [37].

$$k_{2,MEA} = 4.48 \times 10^8 exp\left(-\frac{5400}{T}\right), \ [m^3 \cdot mol^{-1} \cdot s^{-1}] \tag{14}$$

$$k_{Am,DETA} = 7.4692 \times 10^9 exp\left(-\frac{3869.3}{T}\right)$$

$$k_{H_2O,DETA} = 2.0384 \times 10^7 exp\left(-\frac{3450.4}{T}\right), \ [m^6 \cdot kmol^{-2} \cdot s^{-1}] \tag{15}$$

$$k_{2,AEEA} = 1.21 \times 10^4 exp\left[-\frac{3.25 \times 10^4}{R}\left(\frac{1}{T} - \frac{1}{298.15}\right)\right], \ [m^3 \cdot kmol^{-1} \cdot s^{-1}] \tag{16}$$

The reboiler duty is calculated from the reboiler's energy balance; it requires three types of energy: heat of desorption, sensible heat, and latent heat of the amine solvent. The rich amine composition entering the reboiler and the VLE data were determined based on the properties of the liquid and vapor phases in the outlet stream.

The amount of desorbed CO_2 was determined at the reboiler. In the dynamic simulation, it was simpler to monitor the reboiler temperature than the reboiler duty. Therefore, the removal efficiency of CO_2 could be controlled by the reboiler temperature. When the reboiler temperature was determined to achieve the target CO_2 removal efficiency, the composition and flow rate of the outlet stream of the reboiler was also decided. Therefore, the reboiler duty was calculated as the difference between the enthalpies of the inlet and outlet streams of the reboiler directly in the dynamic simulation [47]:

$$Q_{reboiler} = Q_{desorption} + Q_{sensible} + Q_{latent} \tag{17}$$

$$Q_{reboiler} = n_{CO_2}\Delta H_{ab} + nC_p(T_{out} - T_{in}) + n_{H_2O}\Delta H_{H_2O} \tag{18}$$

where $Q_{reboiler}$ is the reboiler duty; $Q_{desorption}$ is the heat of desorption; $Q_{sensible}$ is the sensible heat; Q_{latent} is the latent heat; n is the mass transfer rate; and ΔH_{H_2O} is the latent heat of H_2O.

2.3. Mathematical modeling

The rate-based model was used to predict the fluid behavior inside an absorption column and evaluate the CO_2 capture performance. In addition, the dynamic behavior from the unsteady state to the steady state was predicted when the feed gas composition was changed.

The governing equations for the liquid and vapor phases [48] as well as the mass and energy balance equations are summarized in Table 5. The rate-based model can elucidate the dynamic characteristics from unsteady state to steady state. Furthermore, various rigorous sub-models can be easily employed to the governing equations. In this study, a stripper model consisted of a packing material part, a reboiler part, and a condenser part. Since the material and energy balances at each part could be calculated by reflecting each appropriate input condition, the accuracy for material and energy balance calculation could be enhanced by the rigorous boundary conditions in the liquid phase.

The pressure drop by a liquid hold-up in structured packing was estimated by using Stichlmair's model [49], which was developed from the experiments to measure the liquid hold-up and pressure drop using various viscous fluids. Therefore, in this study, the pressure drop and liquid hold-up in the irrigated packed beds of the absorber and stripper were calculated from the generalized model and relevant equations [49]. Details about the formulas used in the packing column and other units were shown in the appendix.

The mass transfer of liquid and vapor in the structured packing column was predicted by the Rocha's work [50], which was the

Table 5
Governing equations for vapor and liquid phases in absorber and stripper columns.

Expression
Vapor – Continuity
$\frac{\partial(C_t^v(1-h_L))}{\partial t} = -\frac{\partial(C_t^v u_{ve})}{\partial z} - \sum_i n_i^l$
Vapor – Mass balance
$\frac{\partial(C_t^v y_i(1-h_L))}{\partial t} = -\frac{\partial(C_t^v y_i u_{ve})}{\partial z} - n_i^l$
Vapor – Energy balance
$C_t^v(1-h_L)C_p^v\frac{\partial T^v}{\partial t} = -C_t^v C_p^v u_{ve}\frac{\partial T^v}{\partial z} + u_{ve}\frac{dP}{dz} + k_v\frac{\partial^2 T^v}{dz^2} - h_{ov}A_e(T^v - T^l)$
Liquid – Continuity
$\frac{\partial(C_t^l h_L)}{\partial t} = -\frac{\partial(C_t^l u_{le})}{\partial z} + \sum_i n_i^l$
Liquid – Mass balance
$\frac{\partial(C_t^l x_i h_L)}{\partial t} = -\frac{\partial(C_t^l x_i u_{le})}{\partial z} + n_i^l$
Liquid – Energy balance
$C_t^l h_L C_p^l\frac{\partial T^l}{\partial t} = -C_t^l C_p^l u_{le}\frac{\partial T^l}{\partial z} + u_{le}\frac{dP}{dz} + h_{ov}A_e(T^v - T^l) + n_{CO_2}^l A_e \Delta H_{ab} +$
$n_i^l \Delta H_{evap,i}\begin{cases} n_i^l = k_{i,ov}A_e(P_i^v - P_i^{sat}), i = CO_2, H_2O, amine \\ n_i^l = 0, i = N_2, O_2 \end{cases}$

modified model from Bravo's empirical equation [51]. However, instead of the surface area where the vapor and liquid contact each other, an imaginary area, called the effective area, was introduced to enhance the prediction accuracy of the mass transfer. It was reported that the mass transfer model was sufficiently accurate in predicting experimental results using several absorbents [52]. The developed rate-based model was solved using the gPROMS software package (Process Systems Enterprise, UK).

It was assumed that the reaction of amine with CO_2 only occurred in the liquid phase, and those in the vapor phase were neglected. It was also assumed that the mass transfer resistance among H_2O, CO_2, and amine occurred between the liquid and vapor. Then, the mass transfer direction was decided to satisfy Raoult's law. However, the other components (N_2 and O_2) only existed as inert in the vapor phase. The mass transfer rate is determined using the overall mass transfer coefficient:

$$k_{CO_2,ov} = \frac{1}{(RT^v/k_{CO_2}^v) + (H_{CO_2}/k_{CO_2}^l E_{CO_2})} \tag{19}$$

$$k_{i,ov} = \frac{k_i^v}{RT^v},\ i = H_2O, amine \tag{20}$$

where $k_{i,ov}$ is the overall mass transfer coefficient of component i; superscripts v and l are the vapor and liquid phases, respectively; $(k_i^v, k_{CO_2}^v)$ and$k_{CO_2}^l$ are the mass transfer coefficients in the vapor and liquid phases, respectively; H_{CO_2} is Henry's constant of CO_2; and E_{CO_2} is the enhancement factor.

Eq. (17) indicates the effect of both liquid-side and vapor-side resistances on the overall CO_2 mass transfer. The mass transfer coefficient at each phase was obtained using an empirical equation [50]. Because carbamate is formed by the reaction of CO_2 with an amine in the liquid phase, the CO_2 concentration in the liquid phase rapidly decreases. Therefore, the mass transfer coefficient in the liquid phase also affects the overall CO_2 mass transfer rate.

The mass transfer coefficient of CO_2 can be expressed based on the two-film model for a second-order reaction [53]. On the other hand, the mass transfer coefficients for H_2O and amine in the liquid phase were assumed to be negligible [48]. In Eq. (18), the overall mass transfer coefficients of H_2O and amine in the vapor phase are only affected by the component mass transfer coefficient in the vapor phase. The mass transfer coefficient for desorption is calculated using a reference equation [54]:

$$k_i^v = 0.054\frac{D_v}{S}\left(\frac{(u_{ve} + u_{le})\rho_v S}{\mu_v}\right)^{0.8}\left(\frac{\mu_v}{D_v\rho_v}\right)^{0.33},\ i = CO_2, H_2O, amine \tag{21}$$

$$k_{CO_2}^l = 2\left(\frac{0.9D_l u_{le}}{\pi S}\right)^{0.5} \tag{22}$$

where D_v and D_l are the vapor and liquid phase diffusivities, respectively; u_{ve} and u_{le} are the effective velocities in the vapor and liquid phases, respectively; ρ_v is the vapor phase density; and S is the side dimension of the corrugation.

The enhancement factor (E_{CO_2}) in Eq. (17) represents the effect of reactions on the liquid film mass transfer. However, exact theoretical solutions do not exist for second-order kinetics [53]. Hence, in this study, the approximate solution [55] and explicit expression [56] for the enhancement factor of the amine-based absorption process are adopted:

$$E_{CO_2} = \frac{1}{[(1/(E_\infty - 1))^{1.35} + (1/(E_1 - 1))^{1.35}]^{1/1.35}} \tag{23}$$

$$E_\infty = 1 + \left(\frac{C_{amine}^l D_{amine,H_2O}}{2D_{CO_2,amine}C_{CO_2}^v}\right) \tag{24}$$

$$E_1 = 1 + \left(\frac{\sqrt{M}}{tanh\sqrt{M}}\right) \tag{25}$$

$$M = \frac{k_{2,amine}C_{amine}^l D_{CO_2,amine}}{(k_{CO_2}^l)^2} \tag{26}$$

where E_∞ is the instantaneous reaction, and E_1 is the enhancement factor of a pseudo-first-order reaction.

2.4. Parameters for sensitivity study

After the validation of the developed rate-based model, a sensitivity study was conducted using an important parameter: liquid-to-gas ratio (L/G ratio). First, the energy consumption is evaluated according to the change in the L/G ratio, which is the ratio of the amine solvent to the flue gas supplied to the absorber. The optimum L/G ratio for each amine exhibiting the lowest energy consumption is designated as the "baseline condition" for the comparative study. The characteristics of each amine in the absorber and stripper are discussed under the baseline condition.

In the techno-economic analysis of modified absorption processes using MEA in a previous study [13], the increase in capital cost by a RSS configuration was minimal because of the absence of additional devices, whereas the utility energy consumption saving was significant. The RSS configuration supplies a part of the rich amine solvent from the absorber to the top of the stripper without passing through the heat exchanger. In this study, to confirm the feasibility of further energy reduction, the modified absorption process with the RSS (indicated by the red split line) shown in Fig. 1 is also applied to each amine under the baseline condition.

3. Results and discussions

3.1. Validation of a rate-based model

The operational results of the CESAR pilot plant using MEA (Tests 1A-1 to 1A-4) were employed to validate the developed rate-based model. The operating conditions and operating results for Test 1A-1 to 1A-4 were used as the reference values [10,38]. All the packed-bed column properties and operating conditions are summarized in Table 2. Each operation was conducted at different amine flow rates (different L/G ratio). Therefore, the main difference between the Tests was the circulation flow rate of MEA, but, the flue gas input conditions and other process operating conditions were the same. Test 1A-1 was

operated with the highest L/G ratio, and a higher Test number implied a lower L/G ratio.

The temperature profiles inside the absorber are reasonably predicted by the developed model, as shown in Fig. 4(a). Regardless of the flow rate, the temperature increased along the absorber owing to the fast reaction rate and heat of reaction; it then steeply decreased at the top because of the lean amine loading. The lower the L/G ratio, the smaller the temperature rise observed.

The temperature data inside the stripper was available only for Test 1A-1. As shown in Fig. 4(b), the simulated profiles accurately predicted the experimental results. Owing to the condensed solution at the top and the solution from the reboiler at the bottom of the stripper, a relatively steep change in temperature was observed at both ends. The operational results of the pilot plant were reported within the first decimal point digit. Considering the unit of the reboiler duty and the specifications in Table 2, the fluctuation may occur in the second decimal point digit. Therefore, the experimental error bar of the reboiler duty is presented within the second decimal point digit in Fig. 4(c). The simulation results were very similar to Tests 1A-3 and 1A-4 which were operated at low L/G ratios. In Test 1A-2, considering the error bar, the simulation deviation from the pilot plant result was in the range of 0.96 ~ 3.80 %. The simulation result showed a good agreement with the minimum range of the reboiler duty. On the other hand, the simulation result showed a greater deviation at the highest L/G ratio (Test 1A-1), showing 3.01 ~ 5.84 % deviation.

Additionally, the transient test results of the CESAR pilot plant using MEA were employed to validate the dynamic behavior results of the model. The transient test was conducted to examine the system variance when the flow rate of the supplied flue gas was changed from 5000 Nm^3/hr to 3500 Nm^3/hr and other operating variables such as lean amine flow rate or reboiler duty were fixed [39]. As shown in Fig. 4(d), the rate-based model reasonably predicted the experimental CO_2 removal efficiency and CO_2 product flow rate with time after changing the flow gas flow rate. Furthermore, the steady state results could be accurately predicted by the model.

In this study, Test 1A-2 was selected as a comparative reference because the detailed information for the process simulation was available from references [10,38]. In addition, considering that higher amine flow rate than the flow rate at a minimum reboiler duty is practically used in plants, Test 1A-2 was reasonable with respect to safe operation in real operation.

3.2. Sensitivity analysis by L/G ratio

To minimize the reboiler duty, it was essential to adjust the appropriate L/G ratio for each solvent because of the different properties, capacities, and rates of the amines. The sensitivity analysis of the CO_2 capture performance was performed as a function of the L/G ratio for the three amines. The variation in the reboiler duty with the L/G ratio at a constant CO_2 flow rate (Table 2) under the condition that the CO_2 capture exceeds 90% is shown in Fig. 5. At the optimum L/G ratio, DETA had the lowest energy consumption with 3.242 GJ/tonCO_2, followed by MEA with 3.546 GJ/tonCO_2 then AEEA with the highest energy consumption 3.807 GJ/tonCO_2. The optimum L/G ratio to achieve the lowest energy consumption for each amine differs with DETA and MEA exhibiting the lowest and highest L/G ratios, respectively.

Although the CO_2 loading capacity and absorption rate using AEEA were greater than those when MEA was employed (Table 1), the reboiler duty using AEEA was higher than that when MEA was employed; it was also considerably higher than that when DETA was utilized in the entire L/G ratio range (Fig. 5). To analyze the reboiler heat duty, the latent heat of H_2O, CO_2 desorption, and sensible heat are evaluated within the range of the L/G ratio for each solvent. Each energy amount is calculated using Eqs. (15) and (16) for various L/G ratios, and presented by a

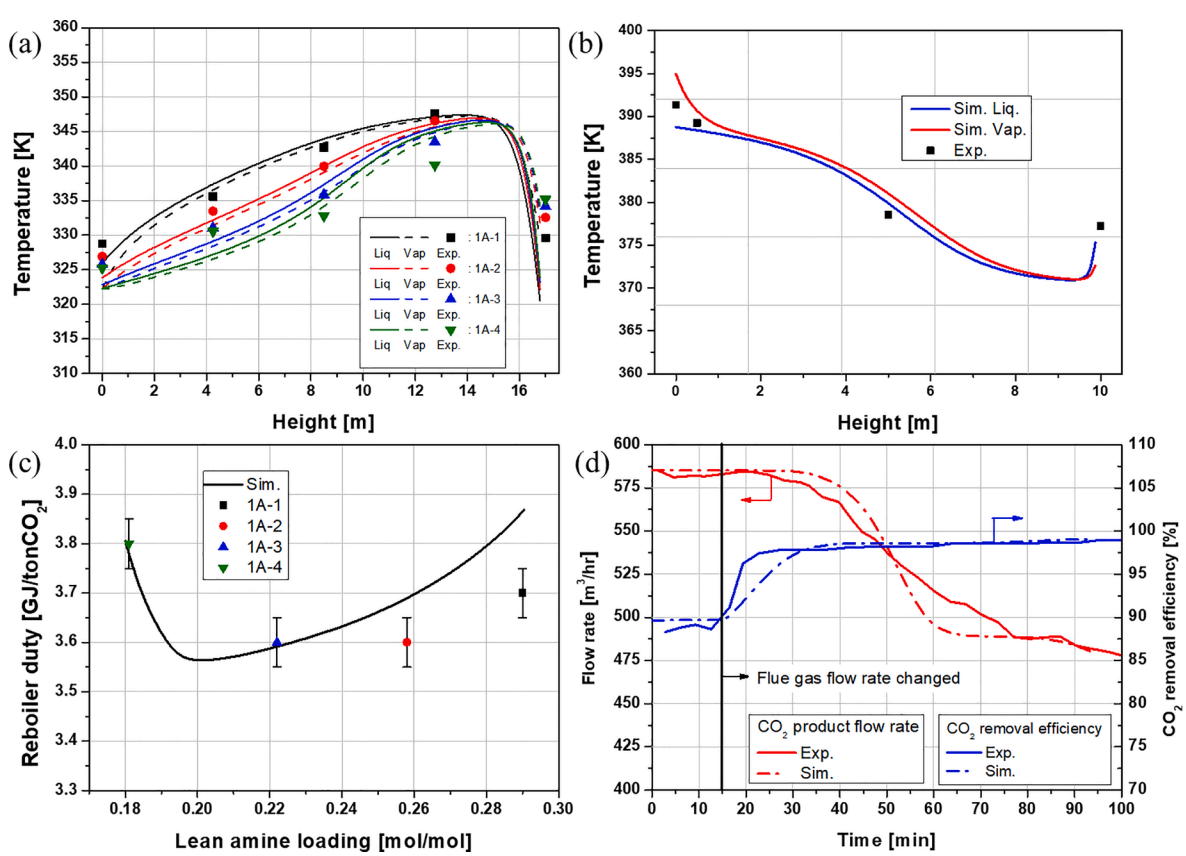

Fig. 4. Comparison between simulation results and literature data [10,38,39] at steady state and dynamic response: temperature profiles in (a) absorber and (b) stripper, (c) reboiler duty, and (d) CO_2 removal efficiency and CO_2 product flow rate.

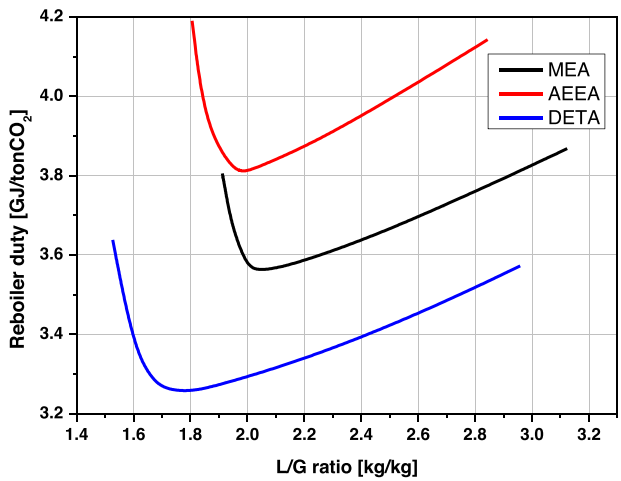

Fig. 5. Variation of reboiler duty as a function of L/G ratio for each amine solvent.

stacked structure in Fig. 6. The sum of the three energy components is the same as the total reboiler duty in Fig. 5. Since too low and too high L/G ratios from the optimum point in Fig. 5 cannot be selected as operating conditions, the figure was presented within a short range of the L/G ratio.

At a lower L/G ratio, more CO_2 per unit mass of amine solvent must be desorbed to achieve a CO_2 capture efficiency exceeding 90%. This indicates that an increase in the reboiler temperature is required; consequently, the amount of vaporized water exceeds the quantity of desorbed CO_2. Because the evaporated water was supplied to the bottom of the stripper and heated the amine solvent, the amount of CO_2 desorbed in the stripper increased. However, this led to a decrease in the amount of CO_2 desorbed in the reboiler. Therefore, when the flow rate of the amine solvent is low, the latent heat of H_2O occupied most of the reboiler duty for all amine solvents.

The contribution of the latent heat of H_2O to the reboiler duty decreases with the increase in the L/G ratio, as shown in Fig. 6. Conversely, at higher amine solvent flow rates, a smaller amount of CO_2 per unit mass of amine solvent could be desorbed, and a smaller amount of steam was generated in the reboiler. Consequently, the heat supplied to the stripper and the amount of CO_2 desorbed in the stripper are reduced, but the amount of CO_2 desorbed in the reboiler is increased. As a result, the heat for CO_2 desorption had the greater proportion in the reboiler duty when the L/G ratio was increased. In addition, as the amount of amine solvent increased, the proportion of sensible heat in the reboiler duty gradually increased with the L/G ratio.

When the amount of CO_2 desorbed per unit mass of amine considerably increased at a lower flow rate of the amine solvent, more energy was required in the reboiler. The contribution of the latent heat of H_2O to the reboiler duty was the highest and decreased with increasing L/G ratio. However, when the flow rate of the amine solvent was extremely high, the reboiler duty gradually increased owing to the increased sensible heat. The contribution of the latent heat of H_2O to the reboiler duty was the highest with AEEA and lowest with DETA.

The difference in the reboiler duty between DETA and AEEA resulted from the desorption efficiency of CO_2 from the reboiler. As shown in Fig. 2, at the operating temperature of the reboiler (~393.15 K), DETA could achieve a lower CO_2 loading compared to AEEA. Therefore, the amount of CO_2 desorption in the reboiler was much greater in DETA. As a result, the CO_2 desorption heat in DETA was higher than that in AEEA, as shown in Fig. 6. Since AEEA could not sufficiently desorb CO_2 in the reboiler at the same condition, a higher temperature for AEEA was required to desorb CO_2 in the stripper. As a result, the latent heat of H_2O

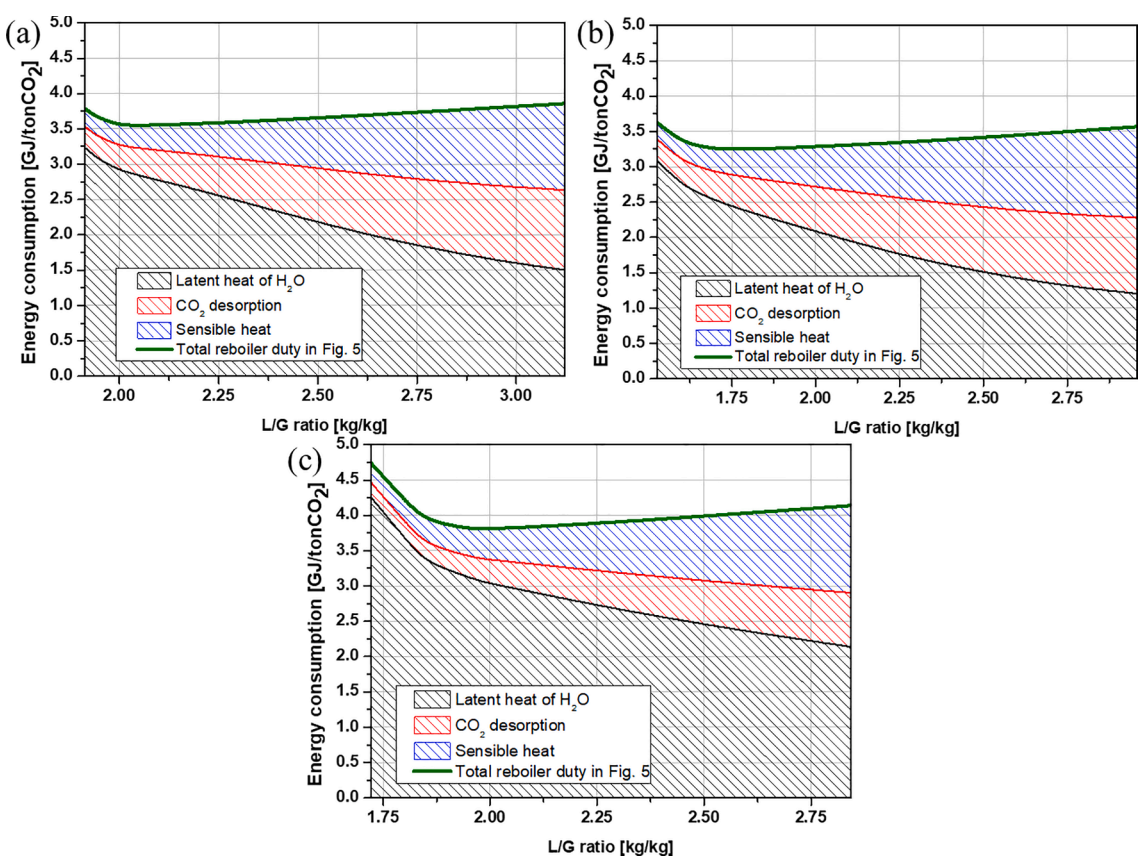

Fig. 6. Contributions of required energy to reboiler heat duty: (a) MEA, (b) DETA, and (c) AEEA.

increased excessively, and the reboiler duty of AEEA was greatly increased. Although the energy consumption of CO_2 desorption was relatively small using AEEA (Fig. 6(c)), its contribution to the overall energy consumption (reboiler duty) was relatively small.

3.3. Comparison with reference process

The profiles inside the absorber using the two multi-amines were compared with those in the absorber using MEA. Because all the amine solvents contained 30 wt% amine (Table 1), the amine mole per solvent mass in DETA and AEEA was smaller than that in MEA because the molecular weights of these two multi-amines were higher. In contrast, because of the two and three amine groups of multi-amines, the number of CO_2 molecules that can react with a mole of amine is higher than that in MEA. Hence, the capacity to capture CO_2 per unit mass of solvent (i.e., DETA and AEEA) was not inferior to the capture capacity using MEA, although the comparison was based on the same weight percentage of amines.

The inside profiles under the baseline condition of each amine (the lowest reboiler duty with the CO_2 capture exceeding 90% (Fig. 5)) are presented in Fig. 7. As shown in Fig. 7(a), the variation in the shape of the mass transfer coefficient along the absorber calculated by Eqs. (17)–(24) is similar regardless of the type of amine; increased coefficient values in the upper sector of the absorber are exhibited. In Fig. 7(a), the mass transfer coefficients of MEA and DETA are similar but higher than those of AEEA.

As summarized in Table 1, the molecular weight, viscosity, CO_2 loading, Henry's constant, and second-order reaction rates differ among the amines; however, other physical properties are similar. According to Eqs. (17)–(24), the higher the amine concentration in the liquid phase, the smaller the Henry's constant and the higher the second-order reaction rate and mass transfer coefficient. Here, the mass transfer coefficient increases in proportion to the power of the second-order rate of 0.5.

In the liquid phase, MEA was found advantageous to Henry's constant and amine concentration (owing to the lowest molecular weight), whereas DETA benefited the second-order reaction rate. As a result, a similar change in the mass transfer coefficient was observed for DETA and MEA. As shown in Fig. 7(b), the CO_2 mole fraction in the vapor phase in the upper sector of the absorber is rapidly reduced in MEA and DETA because of their high mass transfer coefficients. In contrast, the change in CO_2 mole fraction in AEEA was relatively moderate.

The CO_2 mass transfer rate represented the actual rate at which CO_2 changed from gas to liquid phase. It was calculated as the product of the mass transfer coefficient and the difference between the equilibrium and partial pressures. Because MEA and DETA almost reached equilibrium in the upper sector, the mass transfer rate up to the middle sector of the absorber is slower than that of AEEA, as shown in Fig. 7(c). Therefore, as shown in Fig. 7(b), MEA and DETA absorb a large amount of CO_2 in the upper sector of the absorber. However, in the middle sector of the absorber, they absorbed CO_2 more slowly than AEEA.

Fig. 7(d) shows the CO_2 loading for each amine along the absorber. Although the mass transfer rates (or mass transfer coefficients) of DETA and MEA are similar, DETA, with its three amine groups, could capture more CO_2 per mole of amine than MEA. The CO_2 loading distribution along the absorber height are as follows: from 0.556 to 0.202 mol CO_2/mol MEA, from 0.889 to 0.270 mol CO_2/mol AEEA, and from 1.351 to 0.645 mol CO_2/mol DETA. The difference in CO_2 loading between DETA and AEEA was considerably greater than that between AEEA and MEA. Accordingly, each amine solvent was supplied to the stripper at different CO_2 concentrations.

It was expected that the performance of AEEA could be improved by increasing the contact time between the vapor and liquid phases because the mass transfer rate change was small along the absorber. However, in the case of MEA and DETA, the performance was maintained even if the contact time was further reduced. In addition, although the mass

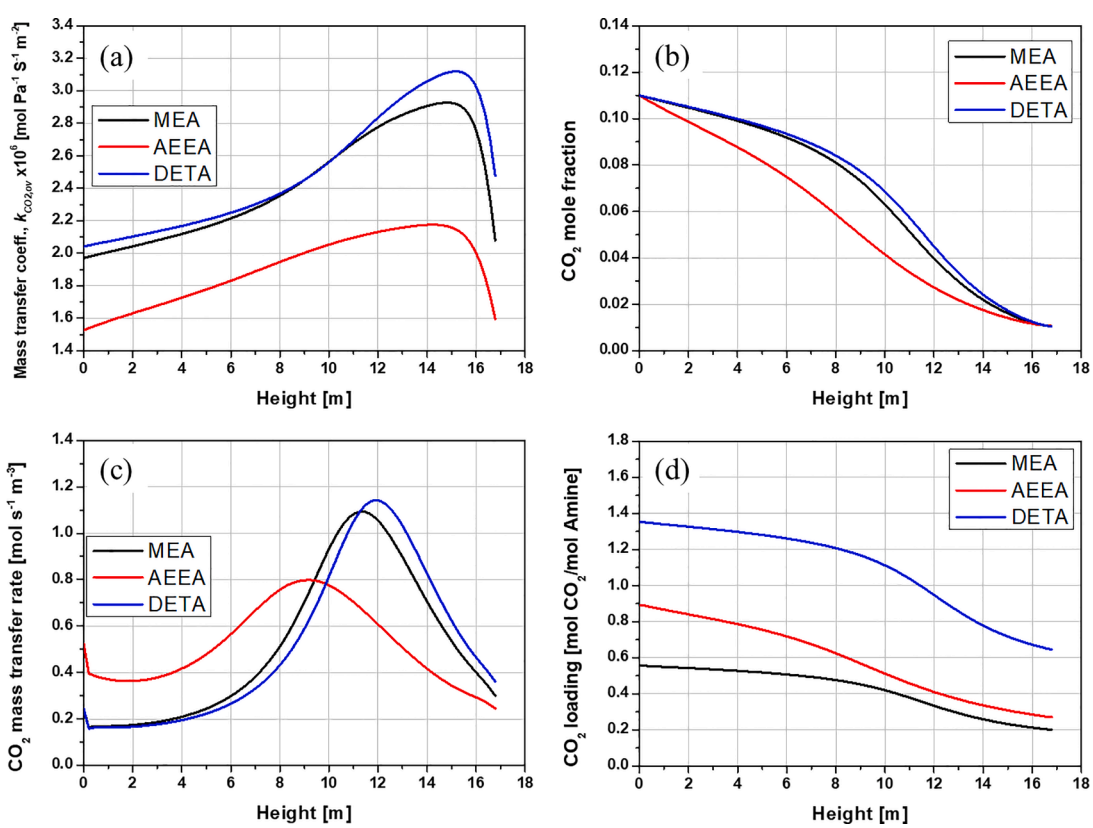

Fig. 7. Comparison of inside profiles among amines in absorber: (a) mass transfer coefficient, (b) CO_2 mole fraction in vapor phase, (c) CO_2 mass transfer rate, and (d) CO_2 loading.

transfer rate of AEEA was slow, increasing the number of amines in the solvent could enhance the CO_2 capture amount in the absorber. However, the energy consumption of the stripper should be carefully evaluated.

The start-up of the absorption process is important for safety and efficient operation. Lean amine at an operating temperature circulates in the absorber and stripper before the flue gas is supplied, and the energy at a set reboiler duty is supplied to the absorption process. Due to a great difference in the properties among the amine solvents, it was expected that the approach from unsteady state to steady state is different among the solvents. The temperature and concentration profiles with respect to time inside the absorber are presented in Fig. 8.

As an initial condition, lean amine without CO_2 loading filled the absorber; hence, lean amine rapidly reacted with CO_2, significantly increasing the temperature. Therefore, when the flue gas was supplied to the absorber, the absorber bottom temperature, where flue gas was supplied, started to rise rapidly (Fig. 8(a)). Then, all the amines exhibited a temperature plateau until 5 min (Fig. 8(b)). Over time, this plateau became shorter. Owing to the faster absorption rate of DETA (Fig. 7(a)), its corresponding temperature plateau was longer than that of the other amines. To approach the steady state, the temperature variation with time was greatest in DETA but lowest in AEEA. Finally, at the steady state, AEEA exhibited the highest temperature variation along the absorber.

As shown in Fig. 8(c), the profile of the CO_2 mole fraction varies with time, i.e., from concave to convex. At 5 min, DETA had the lowest CO_2 mole fraction because of its faster absorption rate. Accordingly, the CO_2 mole fraction in the upper sector of the absorber approached zero. As expected, the CO_2 mole fraction remained low until 15 min (Fig. 8(b)). In addition, the variation in the CO_2 mole fraction with time was the greatest in DETA, whereas AEEA had the smallest mole fraction change with time and the lowest mole fraction along the absorber at the steady state.

Fig. 9 shows the inside-profile of each amine in the stripper. The profiles of the desorption rate and CO_2 flow rate along the stripping packing column (the 10-m packing height in Table 2) are presented in Fig. 9, (a) and (b). In contrast, because the temperature at the washing sector in the stripper is an important factor in the process modification, the temperature of the vapor phase in Fig. 9(c) is in the range of 13 m, which includes the height of the stripping packing column and washing sector.

The mass transfer rate of desorbed CO_2 decreases along the stripper using DETA, as shown in Fig. 9(a). Among the amine solvents, DETA had the fastest CO_2 desorption rate at the bottom sector of the stripper. A large amount of CO_2 was desorbed at the bottom sector of the stripper; hence, a steep decrease in the desorption rate was observed in the middle sector of the stripper with DETA. A slower desorption rate than those of the other amine solvents was observed from the middle to the upper sectors in the stripper. Different from the CO_2 mass transfer rate of the absorber shown in Fig. 7(c), the variation in the shape of the CO_2 desorption rate of AEEA along the stripper is similar to that of MEA, exhibiting a lower desorption rate in the middle sector of the stripper shown in Fig. 9(a).

Because the CO_2 in DETA was well desorbed not only in the stripper but also in the reboiler, a significantly higher CO_2 flow rate in the vapor phase was observed in DETA than in the other amines from the bottom of the stripper (0-m height in Fig. 9(b)), where the CO_2 desorbed from the reboiler was merged. In addition, because DETA had the fastest CO_2 desorption rate in the bottom sector, the flow rate of CO_2 in the vapor phase desorbed from the rich DETA solvent was consistently higher than those of the other amines.

Similar to that in MEA, the CO_2 flow rate in AEEA increased at the

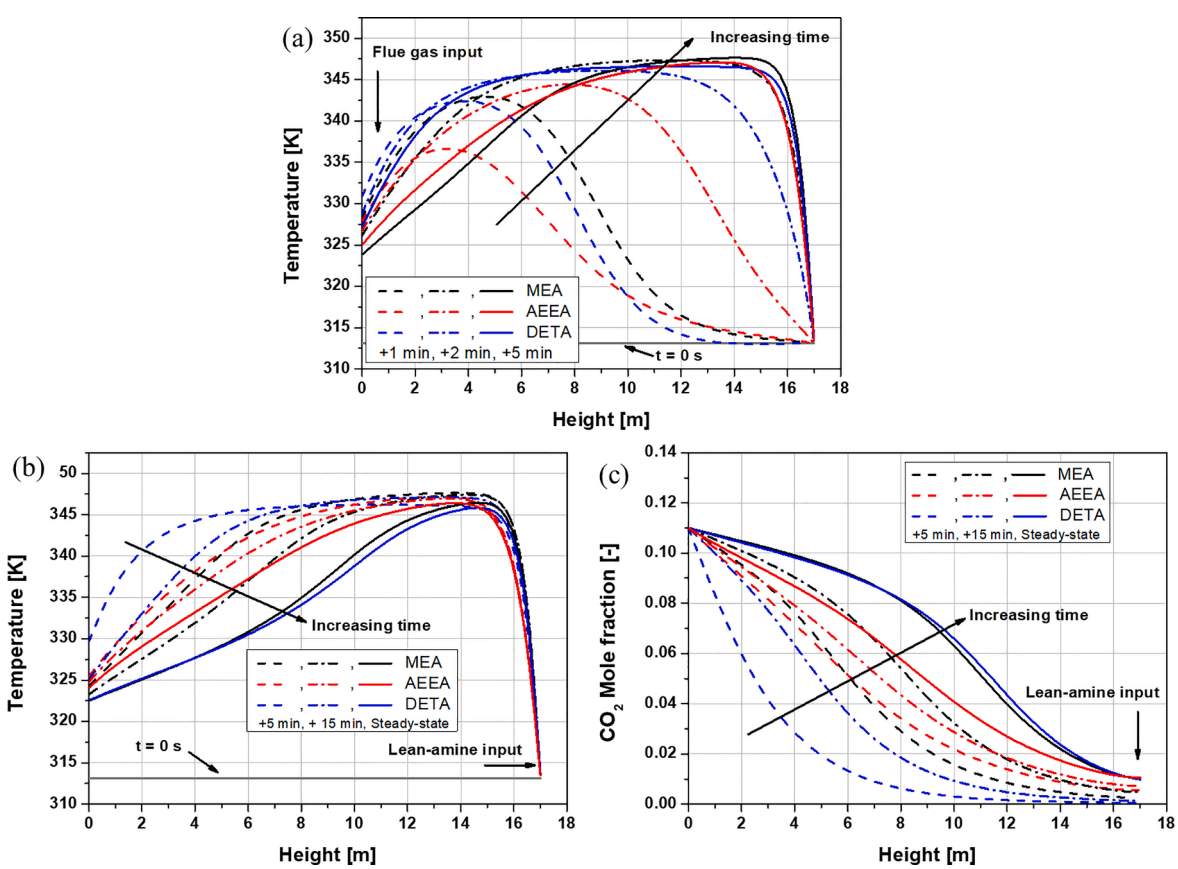

Fig. 8. Dynamic behavior in absorber under baseline condition: (a) Liquid temperature at early time; 1 min, 2 min and 5 min, (b) Liquid-phase temperature and (c) CO_2 mole fraction in vapor phase at 5 min, 15 min, and steady state.

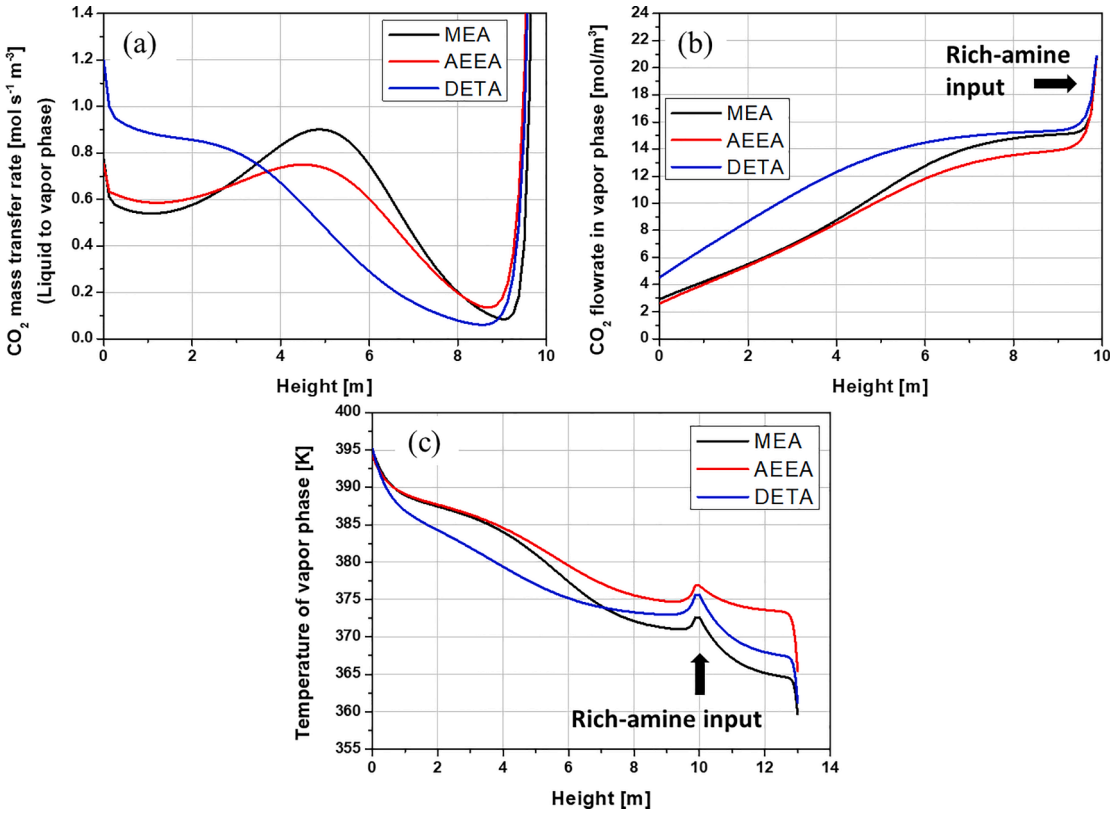

Fig. 9. Comparison of inside profiles in stripper among amines: (a) mass transfer coefficient, (b) CO_2 flow rate in vapor phase, and (c) temperature of vapor phase.

bottom of the stripper because their CO_2 desorption rates were also the same. However, from the middle of the stripper, the CO_2 flow rate became smaller than that of MEA because its CO_2 desorption rate was slower than that of MEA (Fig. 9(a)). Then, the CO_2 flow rate steeply increased at the top of the stripper for all the amines because the CO_2 that was separated from the rich/lean amine heat exchanger entered the stripper.

The temperature of the vapor phase in the stripper is shown in Fig. 9 (c). The operating pressure of the reboiler of all amines was 2 bar, and the VLE state was maintained in the reboiler. Since the reboiler temperature was maintained at 393 ~ 395 K, the highest temperature approached to 395 K (the height of 0 m in Fig. 9(c)). A small temperature evolution at a height of 10 m resulted from the input of the hot rich amine from a rich/lean amine heat exchanger. The temperature decreased along the stripper because of the heat of desorption of CO_2. The fastest decrease in temperature in DETA was observed at the bottom sector of the stripper because it had the fastest CO_2 desorption rate. In contrast, a rapid decrease in the MEA temperature was observed at the middle of the stripper because it had the fastest CO_2 desorption rate in that sector.

Because the desorbed amount of CO_2 in the stripper was smaller using AEEA than using MEA and DETA, the amount of CO_2 desorbed from the reboiler and rich/lean amine heat exchanger must be higher than using MEA and DETA to maintain a CO_2 removal efficiency exceeding 90%. This indicates that the reboiler temperature of AEEA should be increased to achieve lean amine with a lower CO_2 loading. As the temperature of the reboiler increased with AEEA, the temperature of lean amine supplied to the rich/lean amine heat exchanger also increased. Therefore, because of the higher temperature of the rich AEEA solvent, the crossover of the temperature profile with that of DETA was not observed; this was different from that of MEA. The highest temperature of the vapor phase is observed in the washing sector of the stripper, as shown in Fig. 9(c).

When the reboiler temperature with AEEA increased to achieve a CO_2 capture efficiency of 90%, a greater amount of water vapor was generated than the increase in the amount of CO_2 desorption. As shown in Fig. 6(c), the latent heat of H_2O is significantly higher than that of the other two amines, indicating that the highest reboiler duty in the AEEA results from the high latent heat of H_2O.

To reduce the reboiler duty, the target CO_2 loading of the lean amine under the operating conditions of the reboiler was important. If desorption is required to achieve a considerably low CO_2 loading of lean amine, then the reboiler duty significantly increases because of the highly increased latent heat of H_2O by water evaporation. Accordingly, it was confirmed that although the CO_2 loading capacity of the solvents was high, the reboiler duty was not always small.

4. Assessment of process modification

It was reported that the RSS configuration, applied to a conventional absorption process using MEA, could enhance the capture efficiency [12]. In this study, the change in reboiler duty is evaluated when the same RSS configuration as that shown in Fig. 1 (red line) is applied to the absorption process using multi-amines. The split ratio in the RSS configuration indicated that a portion of the rich amine flow was directly supplied to the top of the stripper without passing the rich/lean amine heat exchanger.

An extremely high split ratio was not recommendable because the high amount of vapor generated by the rich amine at excessive heat could endanger the heat exchanger with rich/lean amine [13]. Therefore, when the amine flow rate was increased by 15% and 30% from the baseline condition, the change in reboiler duty was evaluated in the split ratio range from 0.14 to 0.3 (Fig. 11). The decrease in the reboiler duty with DETA is practically linear with the increase in the split ratio, as shown in Fig. 11(a). It was noted that increasing the amine flow rate was advantageous within a certain range of split ratios. The higher the rich amine flow rate applied to the top of the stripper, the more heat energy could be recovered in the washing sector. However, the decrease in the

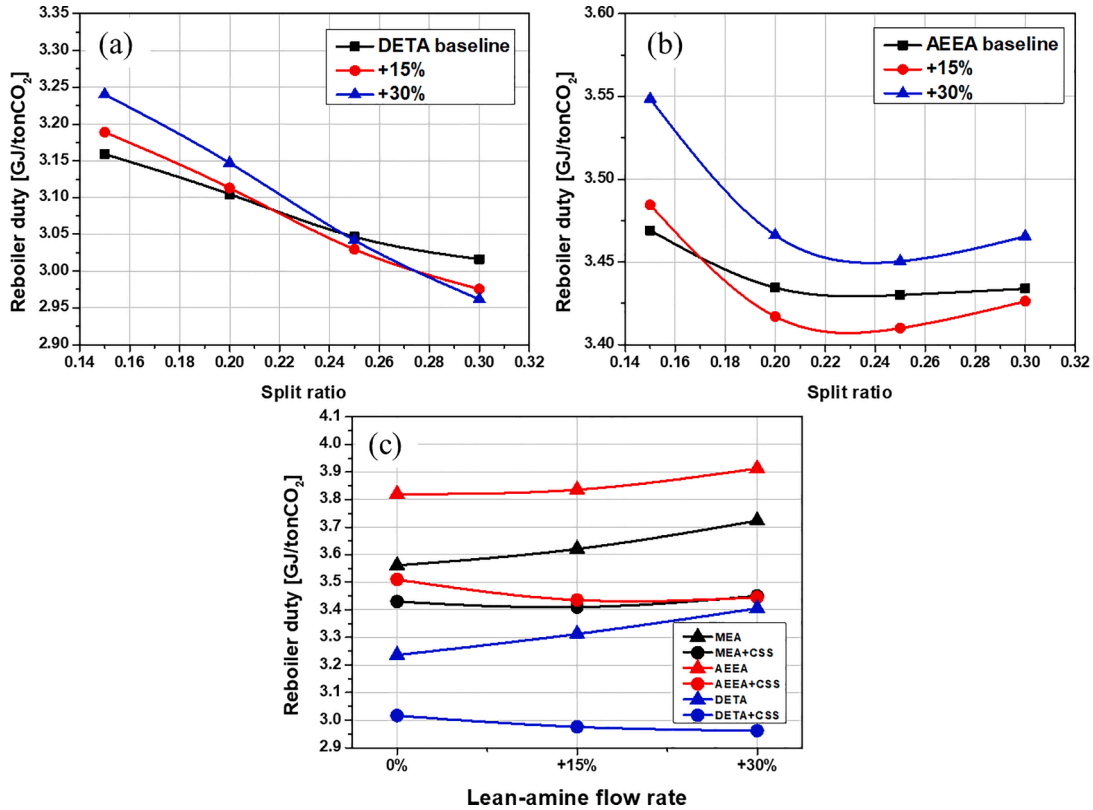

Fig. 11. Reboiler duty at various cold rich split ratios and lean amine flow rates: (a) DETA, (b) AEEA, and (c) comparison between baseline condition and RSS configuration for each amine.

reboiler duty with the increase in the split ratio showed a crossover point among the different amine flowrates. Therefore, the optimum reboiler duty should be carefully selected with DETA according to the available amine flow rate and split ratio.

The reboiler duty with AEEA is reduced with an increase in the split ratio, as shown in Fig. 11(b). However, different from the DETA case, when the split ratio becomes extremely high, the reboiler duty increases because a sufficient amount of amine is not supplied to the rich/lean amine heat exchanger. The decrease in the amount of desorbed CO_2 in the rich/lean amine heat exchanger increases the energy burden of the reboiler. Therefore, the reboiler duty could be minimized from 0.21 to 0.25 of the split ratio by recovering the heat energy of the washing sector. However, the contribution of the CCS configuration to AEEA was smaller than that to DETA.

Fig. 11(c) shows a comparison of the reboiler duty between the baseline condition and RSS configuration when the lean amine flow rate is changed. The RSS configuration can demonstrate the advantage of reducing reboiler duty when rich amine can recover the heat energy from the washing sector to the extent possible. Therefore, as shown in Fig. 11(c), for all the amines, it is observed that the higher the lean amine flow rate, the greater the difference in the reboiler duty between the conventional and CCS configurations. Because the highest temperature at the top of the stripper is used with AEEA, as shown in Fig. 9(c), more heat energy can be recovered by the CCS configuration. The reboiler duty in the CCS configuration using AEEA was similar to that using MEA because the contribution of the CCS configuration to the reboiler duty was the lowest with MEA. The results indicated that the CCS configuration with multi-amines was more effective for CO_2 absorption processes. In this study, the absorption process using DETA achieved the lowest reboiler duty in all cases.

5. Conclusion

The performance of the absorption process using multi-amines for post-combustion CO_2 capture was investigated by developing a rate-based model. The energy efficiency and sensitivity analysis of the absorption process using AEEA and DETA were conducted based on a 90% CO_2 capture and 30 wt% amine solution. The results were compared with those obtained using MEA as the reference solvent.

The reboiler duty of the conventional configuration using DETA was 3.242 GJ/tonCO_2, which was 8.57% lower than that of the MEA process. However, AEEA required more energy in the stripper, resulting from the high energy consumption by the latent heat of H_2O in the reboiler duty even though AEEA had a higher second-order reaction rate and CO_2 loading than MEA. The lower efficiency of AEEA mainly resulted from the slower CO_2 transfer rate in the absorber and stripper than the other amines. Furthermore, the slow CO_2 transfer rate in the absorber can be overcome if sufficient contact time is adopted in the absorber, and higher operating temperatures in the stripper are required for sufficient CO_2 desorption. This required a considerable amount of latent heat of H_2O to increase the temperature, leading to increased energy consumption. It was confirmed that the CO_2 transfer rate in the stripper is a critical performance factor in solvent selection.

In applying the RSS configuration to the absorption process, more energy reduction was observed using the multi-amines than using MEA. DETA could achieve 2.962 GJ/tonCO_2, and even AEEA was able to produce 3.436 GJ/tonCO_2. The process using DETA could reduce the reboiler duty compared with that using MEA with RSS and without RSS by 13.2% and 16.8%, respectively. In the case of the stripper with AEEA operated at a high temperature, the highest reduction in energy consumption of 12.0% was achieved through the RSS configuration.

This study shows that the utilization of a well-selected multi-amine (DETA in this study) in the modified absorption process has considerable potential to increase the energy efficiency of the conventional process.

Additionally, because of the larger molecular weights of DETA and AEEA, the number of their amine molecules present in the 30 wt% amine solution was fewer than the number of amine molecules of MEA. If the mass ratio of multi-amine with a high molecular weight is increased in the solution, then, the energy consumption for CO_2 desorption is reduced. This can be valuable for further performance analysis studies based on the same volume of multi-amines.

CRediT authorship contribution statement

Hyun-Taek Oh: Conceptualization, Methodology, Software, Writing – original draft, Writing – review & editing. **Jae-Cheol Lee:** Validation. **Chang-Ha Lee:** Conceptualization, Writing – review & editing, Supervision.

Declaration of Competing Interest

The authors declare that they have no known competing financial interests or personal relationships that could have appeared to influence the work reported in this paper.

Acknowledgments

This research was supported by the National Research Foundation of Korea (NRF) funded by the Ministry of Science and ICT (2019K1A4A7A03113187).

Appendix A. The equation for rate-based model

A1. Hydrodynamics

The following equations were used to calculated the hydrodynamics in the absorber and stripper columns. The liquid hold-up and pressure drop by a liquid hold-up in structured packing was estimated by using Stichlmair's model [49]:

$$h_0 = 0.555\left(\frac{u_l^2 A_e}{g\varepsilon^{4.65}}\right)^{1/3} \tag{A1}$$

$$h = h_0\left[1 + 20\left(\frac{\triangle P_{irr}}{Z\rho_l g}\right)^2\right] \tag{A2}$$

$$\frac{\triangle P_{dry}}{Z} = \frac{3}{4}f_0\left[\frac{1-\varepsilon}{\varepsilon^{4.65}}\right]\frac{\rho_g u_g^2}{d_p}, f_0 = \frac{C_1}{Re_g} + \frac{C_2}{Re_g^{1/2}} + C_3 \tag{A3}$$

$$\frac{\triangle P_{irr}}{Z} = \frac{\triangle P_{dry}}{Z}\frac{\{1-\varepsilon[1-h/\varepsilon]/(1-\varepsilon)\}^{(2+c)/3}}{(1-h/\varepsilon)^{4.65}} \tag{A4}$$

where h_0 was liquid hold-up below the loading point, u_l was liquid velocity, A_e was effective area, ε was bed porosity, h was liquid hold-up in a packed bed, f_0 was the friction factor for flow past a particle in a bed, C_1, C_2 and C_3 were constant for friction factor, ΔP_{dry} was pressure drop though an unirrigated bed, d_p was particle diameter, and ΔP_{irr} was pressure drop though an irrigated bed.

The effective area was calculated from correlations given by Rocha's work [50]:

$$\frac{A_e}{A_p} = 0.35\frac{29.12(We_l Fr_l)^{0.15}S^{0.359}}{Re_l^{0.2}\varepsilon^{0.6}(1-0.93cos\gamma)(sin\theta)^{0.3}}, cos\gamma = 0.9 \tag{A5}$$

$$We_l = \frac{u_l^2\rho_l S}{\sigma g} \tag{A6}$$

$$Fr_l = \frac{u_l^2}{Sg} \tag{A7}$$

Where A_p was packing surface area, We_l was Weber number for liquid, Fr_l was Froude number for liquid, S was side dimension of corrugation, θ was angle with horizontal for corrugation channel and σ was surface tension.

A2. The flash tank model

The developed two-phase flash tank model was used for the lean solvent cooler, the stripper condenser and reboiler. The developed flash tank model was a zero-dimensional model, and the VLE of the supplied fluids was evaluated according to the operating conditions of the flash tank. At this time, the enthalpy of the input fluid and the output fluid was calculated, respectively. Finally, the heat duty was also evaluated by the difference between the two.

A3. The heat exchanger model

The heat exchanger model was used for a rich/lean solvent heat exchanger. The developed heat exchanger model was also zero-dimensional model, and It was assumed that no reaction occurred. And this model represented the counter-current heat exchanger.

A4. The pipeline model

Since all unit models except the column were zero-dimensional models, there is a disadvantage that the residence time in each unit could not be considered. Therefore, in this study, the pipeline model between each unit was considered, and the residence time in the unit and the time the fluid flows between each unit were also considered. The following equations were used in this model:

$$\frac{dy}{dt} = -\frac{1}{t_r}\frac{dy}{dx} \tag{A8}$$

where y was operating variables, which were flowrate, mole fraction, pressure and temperature, and t_r was the residence time.

This study assumed that the time taken for the fluid from the absorber to be sent to the stripper was 900 s. And the time it takes for the fluid from the stripper to be sent to the absorber is considered to take longer time as 1800 s. This is because it is considered that there is a buffer tank between both columns.

References

[1] International Energy Agency. CO_2 emissions from fuel combustion highlights (2017 edition), https://webstore.iea.org/co2-emissions-from-fuel-combustion/, 2017 [accessed 1 October 2017].

[2] Bui M, Adjiman CS, Bardow A, Anthony EJ, Boston A, Brown S, et al. Carbon capture and storage (CCS): the way forward. Energy Environ Sci 2018;11(5):1062–176.

[3] U.S. DOE Fossil Energy National Energy Technology Laboratory. Carbon Capture Technology Program Plan, January 2013.

[4] Ju Y, Lee C-H. Dynamic modeling of a dual fluidized-bed system with the circulation of dry sorbent for CO_2 capture. Appl Energy 2019;241:640–51.

[5] Jin S, Ko K-J, Lee C-H. Direct formation of hierarchically porous MgO-based sorbent bead for enhanced CO_2 capture at intermediate temperatures. Chem Eng J 2019;371:64–77.

[6] Ju Y, Oh H-T, Lee C-H. Sensitivity analysis of CO_2 capture process in cyclic fluidized-bed with regeneration of solid sorbent. Chem Eng J 2020;379:122291. https://doi.org/10.1016/j.cej.2019.122291.

[7] Oh H-T, Lee W-S, Ju Y, Lee C-H. Performance evaluation and carbon assessment of IGCC power plant with coal quality. Energy 2019;188:116063. https://doi.org/10.1016/j.energy.2019.116063.

[8] Lee WS, Lee JC, Oh HT, Baek SW, Oh M, Lee CH. Performance, economic and exergy analyses of carbon capture processes for a 300 MW class integrated gasification combined cycle power plant. Energy 2017;134:731–42.

[9] Wu X, Wang M, Liao P, Shen J, Li Y. Solvent-based post-combustion CO_2 capture for power plants: A critical review and perspective on dynamic modelling, system identification, process control and flexible operation. Appl Energy 2020;257:113941. https://doi.org/10.1016/j.apenergy.2019.113941.

[10] Razi N, Svendsen HF, Bolland O. Validation of mass transfer correlations for CO_2 absorption with MEA using pilot data. Int J Greenhouse Gas Control 2013;19:478–91.

[11] Sreedhar I, Nahar T, Venugopal A, Srinivas B. Carbon capture by absorption–path covered and ahead. Renewable Sustainable Energy Rev 2017;76:1080–107.

[12] Wilk A, Więcław-Solny L, Tatarczuk A, Krótki A, Spietz T, Chwoła T. Solvent selection for CO_2 capture from gases with high carbon dioxide concentration. Korean J Chem Eng 2017;34(8):2275–83.

[13] Oh H-T, Ju Y, Chung K, Lee C-H. Techno-economic analysis of advanced stripper configurations for post-combustion CO_2 capture amine processes. Energy 2020;206:118164. https://doi.org/10.1016/j.energy.2020.118164.

[14] Lee W-S, Kang J-H, Lee J-C, Lee C-H. Enhancement of energy efficiency by exhaust gas recirculation with oxygen-rich combustion in a natural gas combined cycle with a carbon capture process. Energy 2020;200:117586. https://doi.org/10.1016/j.energy.2020.117586.

[15] Pakzad P, Mofarahi M, Ansarpour M, Afkhamipour M, Lee CH. CO_2 absorption by common solvents. In: Advances in Carbon Capture. 1st ed. Amsterdam: Elsevier; 2020. p. 51–87.

[16] Afkhamipour M, Mofarahi M, Rezaei A, Mahmoodi R, Lee C-H. Experimental and theoretical investigation of equilibrium absorption performance of CO_2 using a mixed 1-dimethylamino-2-propanol (1DMA2P) and monoethanolamine (MEA) solution. Fuel 2019;256:115877. https://doi.org/10.1016/j.fuel.2019.115877.

[17] Svendsen HF, Hessen ET, Mejdell T. Carbon dioxide capture by absorption, challenges and possibilities. Chem Eng J 2011;171(3):718–24.

[18] El Hadri N, Quang DV, Goetheer ELV, Abu Zahra MRM. Aqueous amine solution characterization for post-combustion CO_2 capture process. Appl Energy 2017;185:1433–49.

[19] Kumar S, Mondal MK. Selection of efficient absorbent for CO_2 capture from gases containing low CO_2. Korean J Chem Eng 2020;37(2):231–9.

[20] Bernhardsen IM, Knuutila HK. A review of potential amine solvents for CO_2 absorption process: Absorption capacity, cyclic capacity and pKa. Int J Greenhouse Gas Control 2017;61:27–48.

[21] Afkhamipour M, Mofarahi M, Pakzad P, Lee C-H. Thermodynamic modelling of CO_2 absorption into aqueous solutions of 2-diethylaminoethanol, piperazine, and blended diethylaminoethanol with piperazine. Fluid Phase Equilib 2019;493:26–35.

[22] Afkhamipour M, Mofarahi M, Lee C-H. Thermodynamic Modelling Using e-UNIQUAC Model for CO_2 Absorption by Novel Amine Solutions: 1-dimethylamino-2-propanol (1DMA2P), 3-dimethylamino-1-propanol (3DMA1P) and 4-diethylamino-2-butanol (DEAB). Fluid Phase Equilib 2018;473:50–69.

[23] Liang Z(, Rongwong W, Liu H, Fu K, Gao H, Cao F, et al. Recent progress and new developments in post-combustion carbon-capture technology with amine based solvents. Int J Greenhouse Gas Control 2015;40:26–54.

[24] Han J, Jin J, Eimer DA, Melaaen MC. Density of Water (1) + Monoethanolamine (2) + CO_2 (3) from (298.15 to 413.15) K and Surface Tension of Water (1) + Monoethanolamine (2) from (303.15 to 333.15) K. J Chem Eng Data 2012;57(4):1095–103.

[25] Hartono A, Svendsen HF. Density, viscosity, and excess properties of aqueous solution of diethylenetriamine (DETA). J Chem Thermodyn 2009;41(9):973–9.

[26] Mundhwa M, Alam R, Henni A. Volumetric properties, viscosities, and refractive indices for aqueous 2-((2-aminoethyl) amino) ethanol solutions from (298.15 to 343.15) K. J Chem Eng Data 2006;51(4):1268–73.

[27] Amundsen TG, Øi LE, Eimer DA. Density and Viscosity of Monoethanolamine + Water + Carbon Dioxide from (25 to 80) °C. J Chem Eng Data 2009;54(11):3096–100.

[28] Chiu L-F, Li M-H. Heat Capacity of Alkanolamine Aqueous Solutions. J Chem Eng Data 1999;44(6):1396–401.

[29] Lin S-Y, Leron RB, Li M-H. Molar heat capacities of diethylenetriamine and 3-(methylamino) propylamine, their aqueous binaries, and aqueous ternaries with piperazine. Thermochim Acta 2014;575:34–9.

[30] Mundhwa M, Henni A. Molar heat capacity of various aqueous alkanolamine solutions from 303.15 K to 353.15 K. J Chem Eng Data 2007;52(2):491–8.

[31] Hartono A, Hoff KA, Mejdell T, Svendsen HF. Solubility of carbon dioxide in aqueous 2.5 M of diethylenetriamine (DETA) solution. Energy Procedia 2011;4:179–86.

[32] Ma'mun S, Jakobsen JP, Svendsen HF, Juliussen O. Experimental and Modeling Study of the Solubility of Carbon Dioxide in Aqueous 30 Mass % 2-((2-Aminoethyl) amino)ethanol Solution. Ind Eng Chem Res 2006;45(8):2505–12.

[33] Jou F-Y, Mather AE, Otto FD. The solubility of CO_2 in a 30 mass percent monoethanolamine solution. Can J Chem Eng 1995;73(1):140–7.

[34] Ma'mun S, Svendsen HF.. Solubility of N_2O in aqueous monoethanolamine and 2-(2-Aminoethyl-amino) ethanol solutions from 298 to 343 K. Energy Procedia 2009;1:837–43.

[35] Versteeg G, Van Dijck L, van Swaaij WPM. On the kinetics between CO_2 and alkanolamines both in aqueous and non-aqueous solutions. An overview. Chem Eng Commun 1996;144(1):113–58.

[36] Hartono Ardi, da Silva Eirik F, Svendsen Hallvard F. Kinetics of carbon dioxide absorption in aqueous solution of diethylenetriamine (DETA). Chem Eng Sci 2009;64(14):3205–13.

[37] Ma'mun Sholeh, Dindore Vishwas Y, Svendsen Hallvard F. Kinetics of the reaction of carbon dioxide with aqueous solutions of 2-((2-aminoethyl) amino) ethanol. Ind Eng Chem Res 2007;46(2):385–94.

[38] von Harbou Inga, Imle Michael, Hasse Hans. Modeling and simulation of reactive absorption of CO_2 with MEA: results for four different packings on two different scales. Chem Eng Sci 2014;105:179–90.

[39] Faber Richard, Köpcke Moritz, Biede Ole, Knudsen Jacob Nygaard, Andersen Jimmy. Open-loop step responses for the MEA post-combustion capture process: Experimental results from the Esbjerg pilot plant. Energy Procedia 2011;4:1427–34.

[40] Rao Anand B, Rubin Edward S. Identifying cost-effective CO_2 control levels for amine-based CO_2 capture systems. Ind Eng Chem Res 2006;45(8):2421–9.

[41] Jassim Majeed S, Rochelle Gary T. Innovative absorber/stripper configurations for CO_2 capture by aqueous monoethanolamine. Ind Eng Chem Res 2006;45(8):2465–72.

[42] Lee Woo-Sung, Oh Hyun-Taek, Lee Jae-Cheol, Oh Min, Lee Chang-Ha. Performance analysis and carbon reduction assessment of an integrated syngas purification process for the co-production of hydrogen and power in an integrated gasification combined cycle plant. Energy 2019;171:910–27.

[43] Kim Inna, Svendsen Hallvard F. Heat of Absorption of Carbon Dioxide (CO_2) in Monoethanolamine (MEA) and 2-(Aminoethyl)ethanolamine (AEEA) Solutions. Ind Eng Chem Res 2007;46(17):5803–9.

[44] Kim Inna, Svendsen Hallvard F. Comparative study of the heats of absorption of post-combustion CO_2 absorbents. Int J Greenhouse Gas Control 2011;5(3):390–5.

[45] Frenkel M, Chirico R, Diky V, Kroenlein K, Muzny C, Kazakov A, et al. NIST Standard Reference Database 103b: NIST Thermo-Data-Engine Pure Components, Binary Mixtures, Reactions, version 8.2. Standard Reference Data. Program 2013.
[46] Crooks JE, Donnellan JP. Kinetics and mechanism of the reaction between carbon dioxide and amines in aqueous solution. J Chem Soc Perkin Trans 1989;2:331–3.
[47] Wang R, Liu S, Wang L, Li Q, Zhang S, Chen B, et al. Superior energy-saving splitter in monoethanolamine-based biphasic solvents for CO_2 capture from coal-fired flue gas. Appl Energy 2019;242:302–10.
[48] Jayarathna Sanoja A, Lie Bernt, Melaaen Morten C. Dynamic modelling of the absorber of a post-combustion CO_2 capture plant: Modelling and simulations. Comput Chem Eng 2013;53:178–89.
[49] Stichlmair J, Bravo JL, Fair JR. General model for prediction of pressure drop and capacity of countercurrent gas/liquid packed columns. Gas Sep Purif 1989;3(1):19–28.
[50] Rocha JA, Bravo JL, Fair JR. Distillation columns containing structured packings: a comprehensive model for their performance. 2. Mass-transfer model. Ind Eng Chem Res 1996;35:1660–7.
[51] Bravo JL, Rocha J, Fair J. Mass transfer in gauze packings. Hydrocarb Process 1985;64:91–5.
[52] Afkhamipour Morteza, Mofarahi Masoud. Sensitivity analysis of the rate-based CO_2 absorber model using amine solutions (MEA, MDEA and AMP) in packed columns. Int J Greenhouse Gas Control 2014;25:9–22.
[53] Khan FM, Krishnamoorthi V, Mahmud T. Modelling reactive absorption of CO_2 in packed columns for post-combustion carbon capture applications. Chem Eng Res Des 2011;89(9):1600–8.
[54] Cadours Renaud, Bouallou Chakib, Gaunand Alain, Richon Dominique. Kinetics of CO_2 desorption from highly concentrated and CO_2-loaded methyldiethanolamine aqueous solutions in the range 312–383 K. Ind Eng Chem Res 1997;36(12):5384–91.
[55] Tontiwachwuthikul P, Meisen A, Lim CJ. CO_2 absorption by NaOH, monoethanolamine and 2-amino-2-methyl-1-propanol solutions in a packed column. Chem Eng Sci 1992;47(2):381–90.
[56] Wellek RM, Brunson RJ, Law FH. Enhancement factors for gas-absorption with second-order irreversible chemical reaction. Can J Chem Eng 1978;56(2):181–6.